Performance of Hybrid Adaptive Optics Systems

Michael Werth, Brandoch Calef, Daniel Thompson
The Boeing Company

Stacie Williams, Skip Williams
Air Force Research Laboratory

ABSTRACT

Advances in Adaptive Optics (AO) systems and image processing techniques have allowed image reconstruction to reach new levels of sophistication with impressive improvements in resolvability. The products of these reconstruction methods are often compared by eye due to a lack of widely agreed-upon objective performance metrics. This presentation describes imagery of satellites taken with and without an AO system and with image post-processing. The AO system in question allows for rapid switching between compensated and uncompensated imagery, so an objective comparison between the two is possible. We define and implement a new metric that allows for evaluations of image reconstruction algorithm performance and AO performance.

1. INTRODUCTION

Hybrid Adaptive Optics (HAO) systems combine an Adaptive Optics (AO) system with advanced image processing techniques in order to achieve greater resolution than what is achievable by either system alone. A common goal of new AO system designs and new image processing techniques is to improve the quality of imaging results, and so it becomes necessary to compare the results of one system against another using a set of quality metrics. A good metric is objective, simple to calculate, and provides an easy-to-understand value for image quality. The most common tool used for judging HAO image results has historically been the human eye, which lacks objectivity. The Strehl ratio is the traditional measure of raw AO performance, but it has several shortcomings when applied to HAO: it requires a point source target, which may not be available in scenarios of interest; the image processing stage can oversharpen, leading to exaggerated scores; and under some circumstances the Strehl ratio is not a reliable predictor of subjective image quality [1]. Other metrics such as the Information Theoretic Image Quality Equation (ITIQUE) [2, 3] require a pristine example of the imaging target and are not applicable to evaluation of field data. An objective metric that can be experimentally measured on a wide variety of objects is critical for comparing resolution improvement techniques. One such solution is introduced here.

2. EDGE FITTING TECHNIQUE

When examining the edges of a reconstructed image by eye, one may notice that "better" images tend to have sharply-defined edges. It is possible quantify the quality of edge reconstruction by fitting a parameterized function to the image wherever an object edge is identifiable. We used a simplified form of a generalized logistic function (GLF)

$$GLF(\theta) = A + \frac{B-A}{1+e^{-d(\theta-C)}} \tag{1}$$

for this purpose. This form of the GLF has many advantages. Its lower and upper asymptotes are defined by A and B, respectively. If we renormalize our edge profiles to unity, then these values can be fixed to 0 and 1. The parameter C sets the midpoint of the growth curve, allowing us to fit the function along an axis with arbitrarily-defined units. Parameter d dictates the function's growth rate; flipping the sign of d reverses the function, and as d approaches 0 the slope of the function approaches 0. As d approaches infinity, the function becomes a Heaviside step function, which would be equivalent to a perfectly-defined edge. Examples of the GLF are shown in Fig. 1 below.

1. REPORT DATE **SEP 2013**	2. REPORT TYPE	3. DATES COVERED **00-00-2013 to 00-00-2013**

4. TITLE AND SUBTITLE	5a. CONTRACT NUMBER
Performance of Hybrid Adaptive Optics Systems	5b. GRANT NUMBER
	5c. PROGRAM ELEMENT NUMBER

6. AUTHOR(S)	5d. PROJECT NUMBER
	5e. TASK NUMBER
	5f. WORK UNIT NUMBER

7. PERFORMING ORGANIZATION NAME(S) AND ADDRESS(ES) **The Boeing Company,100 North Riverside ,Chicago,IL,60606**	8. PERFORMING ORGANIZATION REPORT NUMBER

9. SPONSORING/MONITORING AGENCY NAME(S) AND ADDRESS(ES)	10. SPONSOR/MONITOR'S ACRONYM(S)
	11. SPONSOR/MONITOR'S REPORT NUMBER(S)

12. DISTRIBUTION/AVAILABILITY STATEMENT
Approved for public release; distribution unlimited

13. SUPPLEMENTARY NOTES
2013 AMOS (Advanced Maui Optical and Space Surveillance) Technical Conference, 10-13 Sep, Maui, HI.

14. ABSTRACT
Advances in Adaptive Optics (AO) systems and image processing techniques have allowed image reconstruction to reach new levels of sophistication with impressive improvements in resolvability. The products of these reconstruction methods are often compared by eye due to a lack of widely agreed-upon objective performance metrics. This presentation describes imagery of satellites taken with and without an AO system and with image post-processing. The AO system in question allows for rapid switching between compensated and uncompensated imagery, so an objective comparison between the two is possible. We define and implement a new metric that allows for evaluations of image reconstruction algorithm performance and AO performance.

15. SUBJECT TERMS

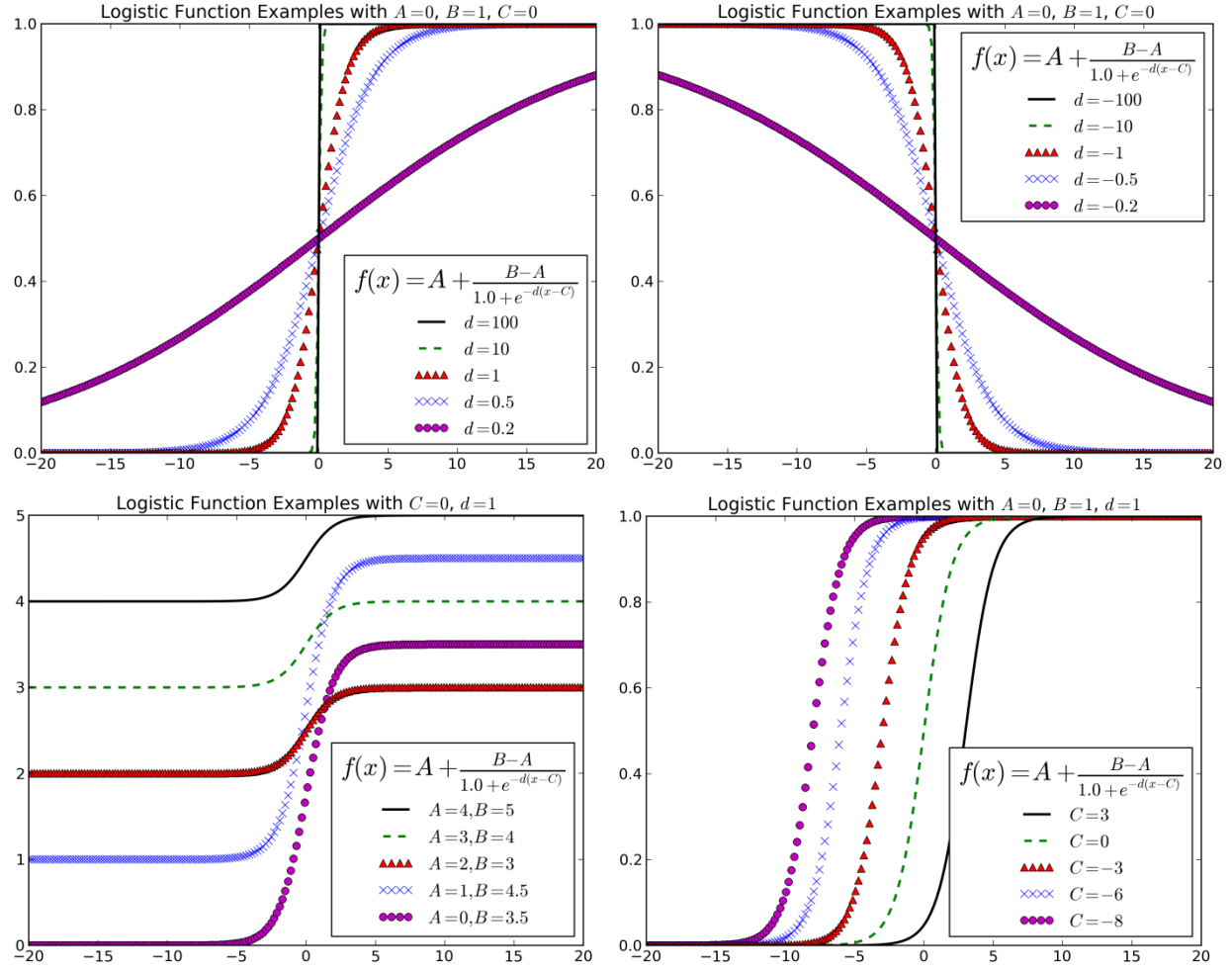| 16. SECURITY CLASSIFICATION OF:			17. LIMITATION OF ABSTRACT	18. NUMBER OF PAGES	19a. NAME OF RESPONSIBLE PERSON
a. REPORT **unclassified**	b. ABSTRACT **unclassified**	c. THIS PAGE **unclassified**	**Same as Report (SAR)**	**9**	

Fig. 1. Examples of logistic functions with varied parameters. Parameters A, B, and C determine the lower asymptote, the upper asymptote, and the growth midpoint of the curve, respectively. Parameter d determines the slope of the curve at the growth midpoint and is the parameter of primary interest; a large absolute value of d indicates a sharply defined edge.

The GLF in Eqn. 1 is the line spread function (LSF) convolved with a Heaviside Function with its step located at $\theta = C$. By deconvolving the two, it becomes possible to measure the full width at half maximum (FWHM) of the LSF and to compare that to the diffraction-limited LSF's FWHM. This deconvolution can be performed in Fourier space:

$$GLF(\theta) = LSF(\theta) \otimes H(\theta - C) \tag{2}$$

$$LSF(\theta) = \mathcal{F}^{-1}\left\{\frac{\mathcal{F}[GLF(\theta)]}{\mathcal{F}[H(\theta-C)]}\right\}. \tag{3}$$

From Eqn. 3, one can obtain the experimentally-measured FWHM of the LSF. The FWHM of the diffraction-limited LSF is also of interest for comparative reasons. This is obtained by integrating the diffraction-limited point-spread function

$$PSF(R) = 4\left(\frac{J_1(\pi R)}{\pi R}\right)^2 \tag{4}$$

along one axis [4]:

$$LSF(x) = \frac{3}{4}\int_0^\infty \left(\frac{J_1\left(\pi\sqrt{x^2+y^2}\right)}{R}\right)^2 dx. \qquad (5)$$

Eqn. 5 has no analytical form, but it can be numerically integrated. Doing this, one finds that the FWHM of the LSF is about λ/D. The diffraction-limited FWHM of a 3.6m telescope observing light with wavelength 800nm is

$$\theta_{\text{FWHM}} = \frac{\lambda}{D} = 0.046". \qquad (6)$$

3.   EXTENDED OBJECT EDGE FITTING

The AEOS 3.6m telescope was used to produce calibrated observations of several extended objects with and without the AO system. Objects were post-processed with a physically constrained iterative deconvolution (PCID) image reconstruction algorithm [5,6] or a faster but less accurate version of this algorithm (PCID_Fast). After calibrating the image, additional bias subtraction is applied: a box of pixels with length equal to 20% of the full frame size is taken from each corner of the image, the median of each box is calculated, and the minimum of these medians is subtracted from the image. Next, one or more edges were identified for each image, and nearest-neighbor interpolation was used to define a light curve along pixels that were perpendicular to each edge. The edge profile was smoothed with a Hamming window and then renormalized so that its minimum and maximum values are 0 and 1 respectively. The generalized logistic function in Eqn. 1 is then fit to the curve while constraining the values of A and B to 0 and 1, respectively. A LSF was extracted from each GLF using Eqns. 2-4, and then the FWHM of the LSF before compensation or processing (AO or PCID) was compared to the FWHM of the LSF after compensation or processing.
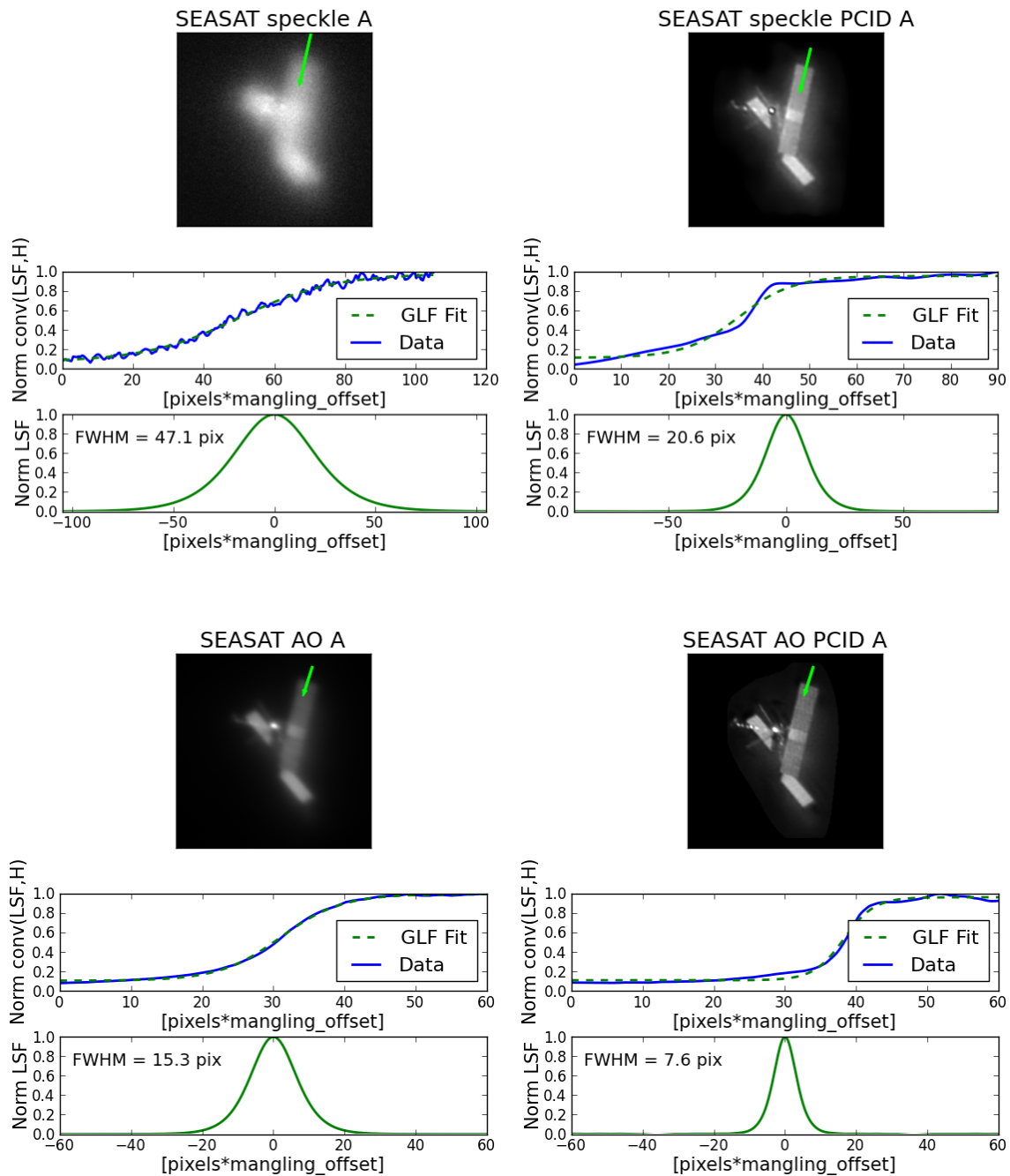
Fig. 2. SEASAT was recorded with an AO system turning on and off in five second intervals. Raw and AO-compensated images were separately processed using a PCID image reconstruction algorithm. The LSF was extracted along a randomly chosen edge and the FWHM was evaluated for each of the above images. These images, with the analysis on the upper edge, are referred to as SEASAT A.
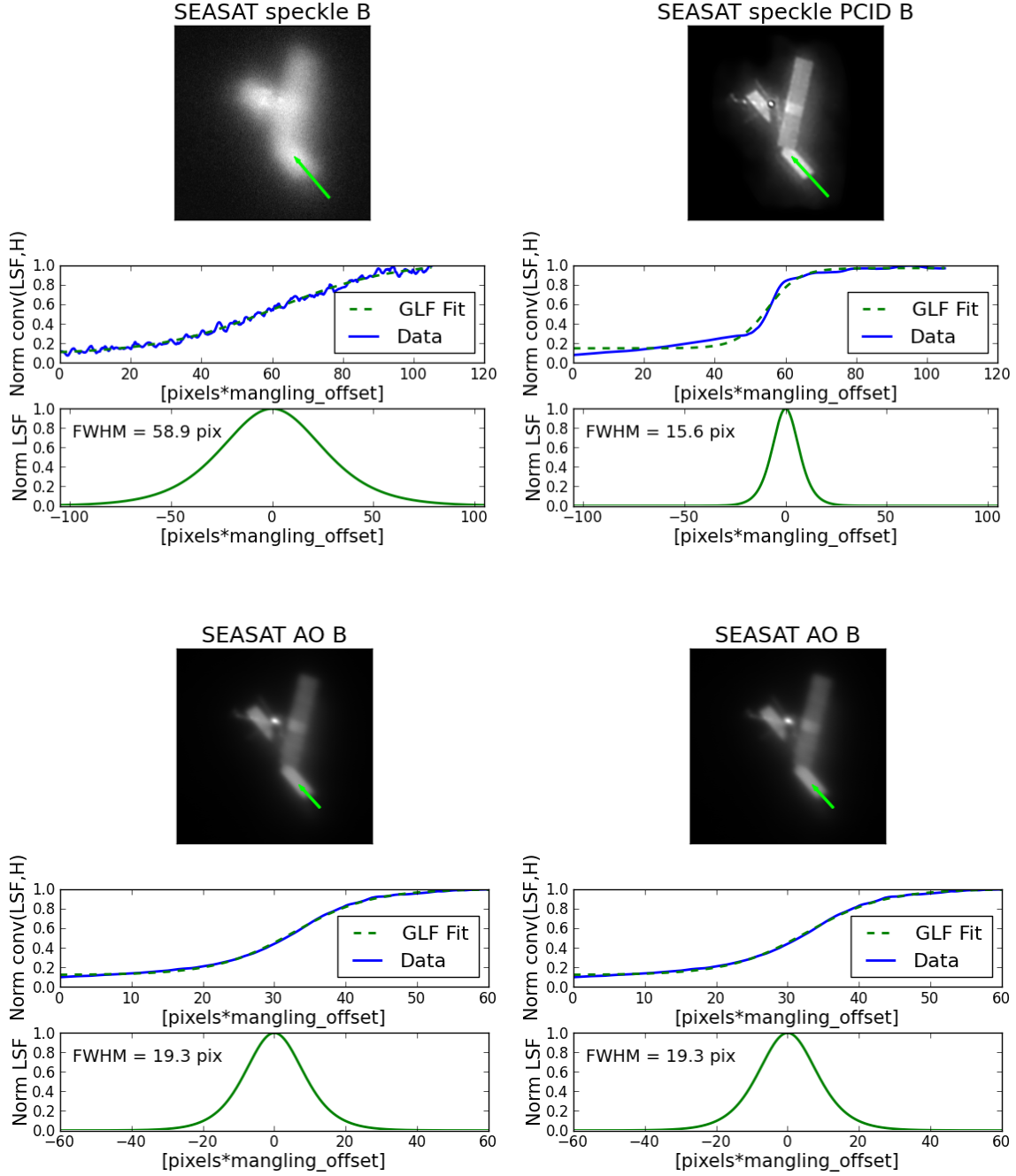
Fig. 3. SEASAT was recorded with an AO system turning on and off in five second intervals. Raw and AO-compensated images were separately processed using a PCID image reconstruction algorithm. The LSF was extracted along a randomly chosen edge and the FWHM was evaluated for each of the above images. This figure is identical to Fig. 2 except for the choice of a different edge. These images, with the analysis on the lower edge, are referred to as SEASAT B.
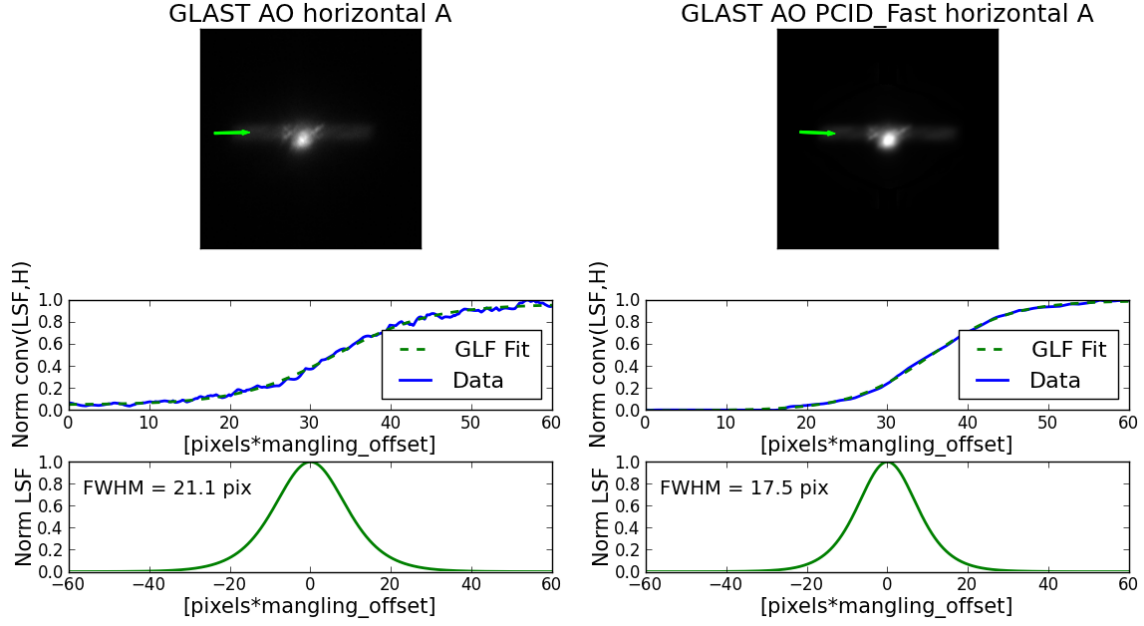
Fig. 4. GLAST was recorded with an AO system. AO-compensated images were processed using a fast version of the PCID image reconstruction algorithm. The LSF was extracted along a randomly chosen edge and the FWHM was evaluated for each of the above images. These images, with the analysis on the left edge, are referred to as GLAST HORIZONTAL A.

Fig. 5. GLAST was recorded with an AO system. AO-compensated images were processed using a fast version of the PCID image reconstruction algorithm. The LSF was extracted along a randomly chosen edge and the FWHM was evaluated for each of the above images. These images, with the analysis on the right edge, are referred to as GLAST HORIZONTAL B.

GLAST AO vertical A

GLAST AO PCID_Fast vertical A
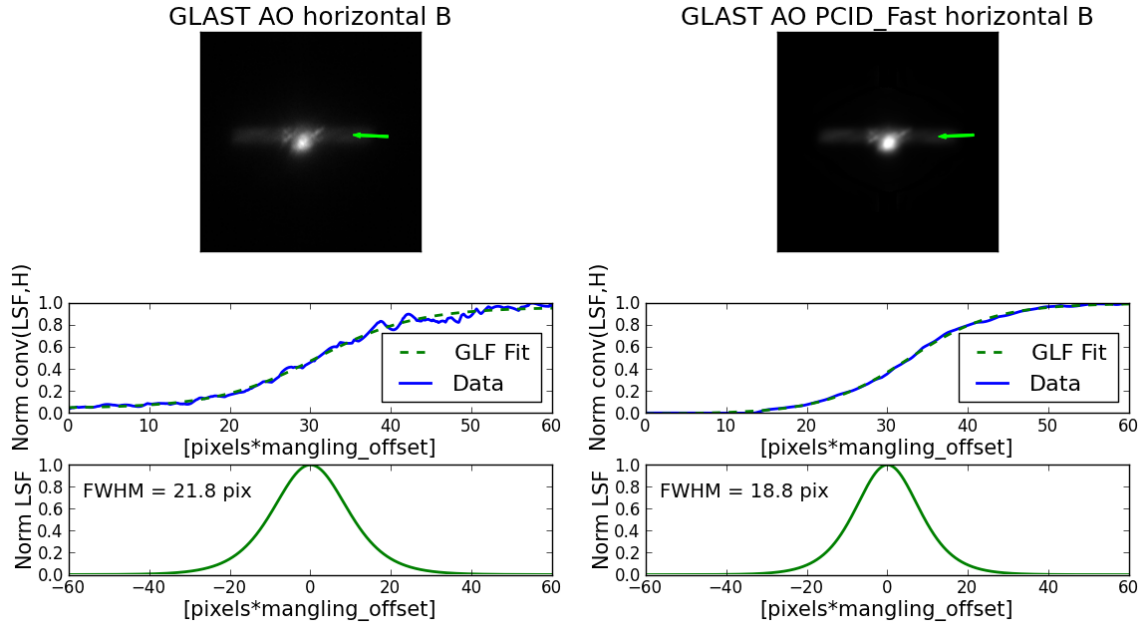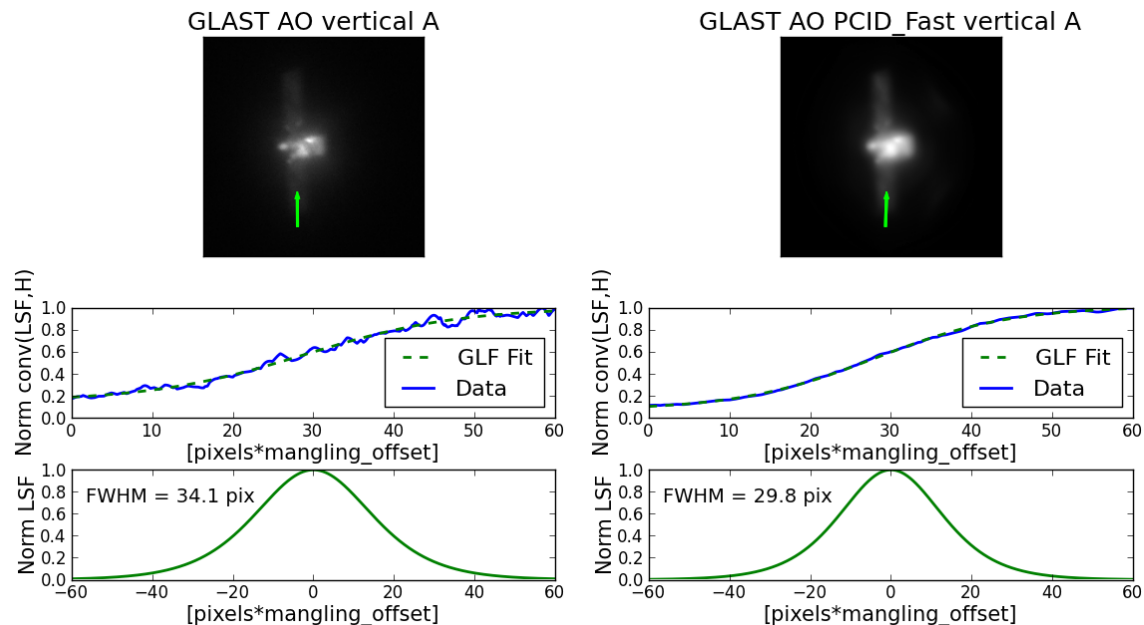
FWHM = 34.1 pix

FWHM = 29.8 pix

Fig. 6. GLAST was recorded with an AO system. AO-compensated images were processed using a fast version of the PCID image reconstruction algorithm. The LSF was extracted along a randomly chosen edge and the FWHM was evaluated for each of the above images. These images, with the analysis on the lower edge, are referred to as GLAST VERTICAL A.

GLAST AO vertical B

GLAST AO PCID_Fast vertical B
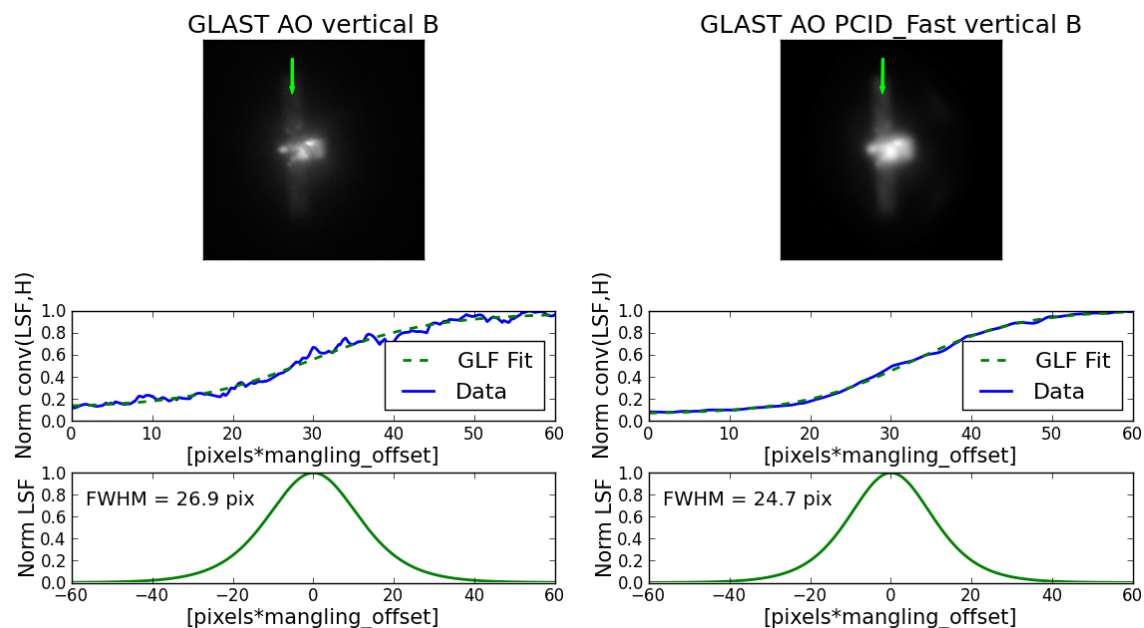
FWHM = 26.9 pix

FWHM = 24.7 pix

Fig. 7. GLAST was recorded with an AO system. AO-compensated images were processed using a fast version of the PCID image reconstruction algorithm. The LSF was extracted along a randomly chosen edge and the FWHM was evaluated for each of the above images. These images, with the analysis on the upper edge, are referred to as GLAST VERTICAL B.

Satellite	Uncompensated FWHM	AO compensated FWHM	Improvement
SEASAT A	47	15	3.1
SEASAT B	59	19	3.1
SEASAT A + PCID	21	7.6	2.7
SEASAT B + PCID	16	9.3	1.7

Table 1. AO performance was evaluated by looking at the ratio of LSF FWHM with AO compensation to the LSF FWHM without compensation. SEASAT was observed with an AO system turning on and off in five second intervals. This allowed us to examine the relative improvement that the AO system brings to edge resolution. Without PCID reconstruction, the AO system consistently provided about a factor of 3 improvement in resolution between the two examined edges over uncompensated imagery. SEASAT B uses a position that appears to be more susceptible to dispersion effects than SEASAT A, which results in a discrepancy between the improvement ratios of panel A and B with PCID reconstruction versus AO + PCID reconstruction.

Satellite	Unprocessed FWHM	PCID-processed FWHM	Improvement
SEASAT A RAW	47	21	2.2
SEASAT B RAW	59	16	3.7
SEASAT A AO	15	7.6	2.0
SEASAT B AO	19	9.3	2.0
GLAST HORIZONTAL A AO	21	18	1.2
GLAST HORIZONTAL B AO	22	19	1.2
GLAST VERTICAL A AO	34	30	1.1
GLAST VERTICAL B AO	27	25	1.1

Table 2. PCID performance was evaluated by examining the ratio of LSF FWHM before and after PCID image reconstruction was applied. SEASAT images were processed with a PCID reconstruction algorithm and GLAST images were processed with a faster version of the PCID algorithm. The GLAST images in the vertical orientation were observed at a lower elevation angle than the GLAST images in the horizontal orientation; this may explain why the achieved edge resolution is slightly worse for the vertical orientation.

4. CONCLUSIONS

We have presented early development of a metric that can be used in evaluating the edge reconstruction resolution of an imaging system. This metric involves taking the distribution of counts passing through a line perpendicular to the edge of an object, fitting this distribution to a logistic function, deconvolving the result from a Heaviside function, and then extracting the FWHM from the resulting LSF. This method is objective and consistent between the tested objects, and the choice of edge does not appear to strongly influence the estimated FWHM. The AEOS 3.6m AO system was found to consistently provide an edge resolution improvement of at least 3.0 over uncompensated imagery, the PCID reconstruction algorithm was found to provide edge resolution improvements

between 1.3 and 2.0 over unprocessed imagery, and the PCID_Fast reconstruction algorithm was found to provide edge resolution improvements of 1.1 to 1.2 over AO-compensated imagery.

In future work, taking the mean or median of counts along thicker line segments could help to reduce noise influence. Observing a large number of extended objects with a variety of elevation angles and seeing conditions would help in further understanding the achievable edge resolution of the AEOS HAO imaging system. Comparing this metric to other commonly-used metrics, such as Sharpness and Variance of Laplacian of Gaussian, would also be useful in assessing the pros and cons of using this new edge-based metric.

5. REFERENCES

1   Brigantic, R.T., Roggemann, M.C., Bauer, K.W., and Welsh, B.M., *Image-quality metrics for characterizing adaptive optics system performance*, Applied Optics, Vol. 36, No. 26, 6583-6593, 1997.
2   Gerwe, D.R., Luna, C.E., and Calef, B., *Information Theoretic Based Image Quality Evaluation*, OSA Signal and Recovery Conference STuC1, 2009.
3   Gerwe, D.R., Luna, C.E., and Calef, B., *Application of the ITIQUE Image Quality Metric to SSA Domain Imagery*, Advanced Maui Optical and Space Surveillance Technologies Conference, 2012.
4   Smith, W.J., *Modern Optical Engineering*, McGraw-Hill, 2000.
5   Matson, C.L. et al, *PCID and ASPIRE 2.0 – the next generation AMOS image processing environment*, Advanced Maui Optical and Space Surveillance Technologies Conference, 2007.
6   Matson, C.L. et al, *Fast and optimal multiframe blind deconvolution algorithm for high-resolution ground-based imaging of space object*, Applied Optics, Vol. 48, A75-A92, 2009.